Journal of Molecular Graphics and Modelling 29 (2011) 996–1005

Contents lists available at ScienceDirect

Journal of Molecular Graphics and Modelling

journal homepage: www.elsevier.com/locate/JMGM

# Binding conformation prediction between human acetylcholinesterase and cytochrome *c* using molecular modeling methods

Songmi Kim[a], Yuno Lee[a], Prettina Lazar[a], Minky Son[a], Ayoung Baek[a], Sundarapandian Thangapandian[a], Na Young Jeong[b], Young Hyun Yoo[b], Keun Woo Lee[a,*]

[a] *Division of Applied Life Science (BK21 Program), Research Institute of Natural Science (RINS), Plant Molecular Biology and Biotechnology Research Center (PMBBRC), Gyeongsang National University, Jinju 660-701, Republic of Korea*
[b] *Department of Anatomy and Cell Biology, Dong-A University College of Medicine and Medical Science Research Center, Busan 602-714, Republic of Korea*

ARTICLE INFO

*Article history:*
Received 7 January 2011
Received in revised form 15 April 2011
Accepted 18 April 2011
Available online 27 April 2011

*Key words:*
Acetylcholinesterase (AChE)
Cytochrome *c* (Cyt *c*)
Macro-molecular docking study
Protein–protein docking simulation
Molecular dynamics (MD) simulation

ABSTRACT

The acetylcholinesterase (AChE) is important to terminate acetylcholine-mediated neurotransmission at cholinergic synapses. The pivotal role of AChE in apoptosome formation through the interactions with cytochrome *c* (Cyt *c*) was demonstrated in recent study. In order to investigate the proper binding conformation between the human AChE (hAChE) and human Cyt *c* (hCyt *c*), macro-molecular docking simulation was performed using DOT 2.0 program. The hCyt *c* was bound to peripheral anionic site (PAS) on hAChE and binding mode of the docked conformation was very similar to the reported crystal structure of the AChE and fasciculin-II (Fas-II) complex. Two 10 ns molecular dynamics (MD) simulations were carried out to refine the binding mode of docked structure and to observe the differences of the binding conformations between the absent (Apo) and presence (Holo) of heme group. The key hydrogen bonding residues between hAChE and hCyt *c* proteins were found in Apo and Holo systems, as well as each Tyr341 and Trp286 residue of hAChE was participated in cation-pi ($\pi$) interactions with Lys79 of hCyt *c* in Apo and Holo systems, respectively. From the present study, although the final structures of the Apo and Holo systems have similar binding pattern, several differences were investigated in flexibilities, interface interactions, and interface accessible surface areas. Based on these results, we were able to predict the reasonable binding conformation which is indispensable for apoptosome formation.



## 1. Introduction

Acetylcholinesterase (AChE) is important for terminating acetylcholine-mediated neurotransmission at cholinergic synapses and it catalyzes the hydrolysis of acetylcholine at cholinergic synapses as well as at neuromuscular junctions [1,2]. The AChE has influence on various physiological processes relative to the regulation of cell proliferation, differentiation and survival [3]. There are three different isoforms by alternative splicing at C-terminus of AChE mRNA. It is called AChE-R (read-through), AChE-E (erythrocytic) and AChE-S or T (synaptic or tail) based on the place of expression. AChE-R variant is expressed in embryonic and tumor cells and induced in response to chemical, psychological and physical stresses included AChE inhibition. AChE-E is linked to glycosylphosphatidyl inositol (GPI). This lipid moiety may be integrated into erythrocyte membrane and anchor the mature AChE-E to the outer surface of erythrocytes [3,4]. AChE-S variant expressed in the brain and muscles of normal adult mammals and generate a monomer, dimer and several polymeric forms included tetramers [5–7]. In vertebrate cholinergic synapses, four AChE-S monomers aggregate with collagen like Q subunit (ColQ) or transmembrane proline-rich memebrane-anchoring protein (PRiMA) to form a tetramer [8]. The crystal structures of AChE are characterized from *Torpedo californica* [9], *Drosphila malanogaster* [10], *Mus musculus* [11], and *Homo sapiens* [12,13]. The narrow and deep gorge of the structures can be found with consisting of two separate ligand binding sites such as acylation site and peripheral anionic site (PAS). The acylation site containing a catalytic triad is located at the bottom of the gorge and the PAS lies at the top of the gorge [13,14] (Fig. 1A and B). Several studies revealed that the active site of hAChE can be distinguished into several subsites such as catalytic triad (Ser203, His447, and Glu334), oxyanion hole (Gly121, Gly122, and Ala204), anionic subsite (Trp86, Tyr133, Glu202, Gly448, and Ile451), acyl binding pocket (Trp236, Phe295, Phe297, and Phe338), and PAS (Asp74, Tyr124, Ser125, Trp286, Tyr337, and Tyr341) [13,15–19].

According to several experimental studies, AChE is potentially a marker and a regulator of apoptosis [20] and it also plays a pivotal role in apoptosome formation [21]. Moreover, a recent study demonstrated that interactions of AChE with caveolin-1 (Cav-1)

* Corresponding author. Tel.: +82 55 751 6276; fax: +82 55 752 7062.
*E-mail address:* kwlee@gnu.ac.kr (K.W. Lee).

1093-3263/$ – see front matter © 2011 Elsevier Inc. All rights reserved.
doi:10.1016/j.jmgm.2011.04.006

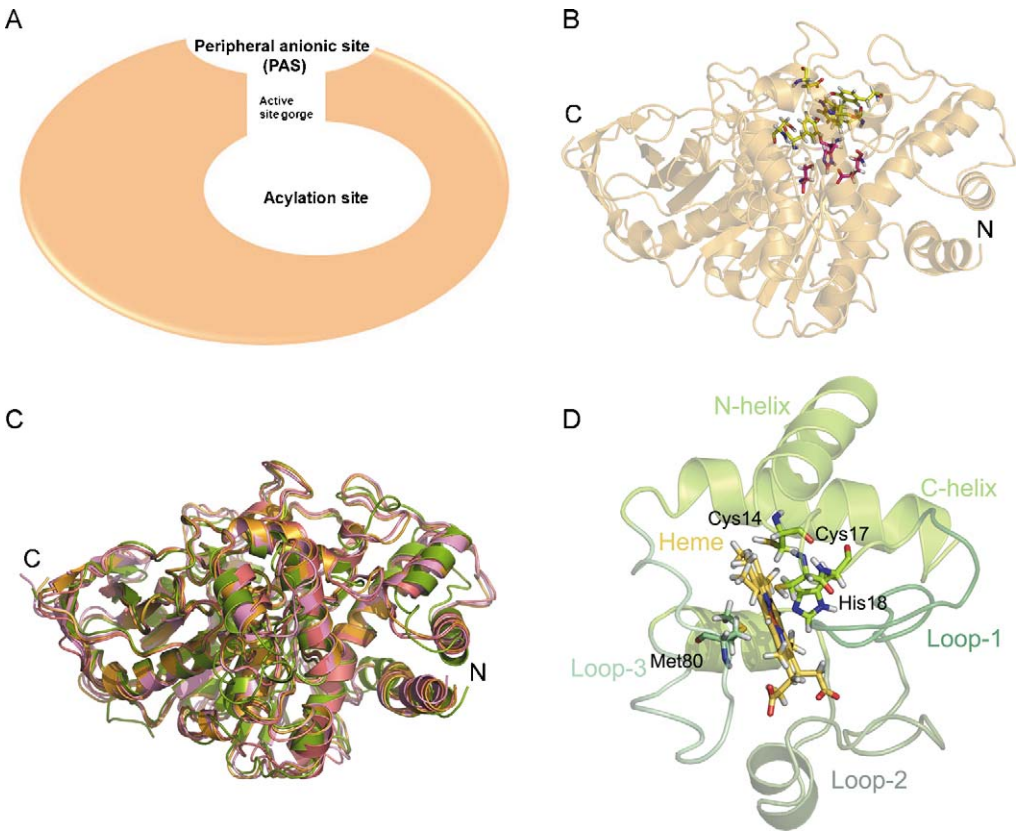


**Fig. 1.** Structural features of hAChE and structural elements of hCyt *c*. (A) Schematic representation of the sites in hAChE. (B) The catalytic triad (magenta) and peripheral anionic site (PAS) residues (yellow) in the structure of hAChE [PDB ID: 1B41] displayed as sticks. (C) Superimposition of AChE structures with various sources (orange for *homo sapiens*, pink for *Mus musculus*, deep-salmon for *Torpedo californica*, and split-pea for *Drosophila melanogaster*). (D) Structure elements (green for helices, stmudge for loop1, pale-green for loop2, and forest for loop3) in the 3D structure of the hCyt *c* [PDB ID: 1J3S] with heme group (yellow) and heme binding residues represented as stick. (For interpretation of the references to color in this figure legend, the reader is referred to the web version of the article.)

and subsequently with cytochrome *c* (Cyt *c*) are required for apoptosome formation. It was suggested that silencing of the *AChE* gene blocked the interaction between apoptotic protease-activating factor-1(Apaf-1) and Cyt *c*. Furthermore, they indicated that the interaction between AChE and Cyt *c* is required for the interaction between Cyt *c* and Apaf-1 through silencing of *cytochrome c* gene [21,22]. Generally, Cyt *c* is an electron carrier and heme group be able to attach to CXXCH motif which is heme binding sites in the Cyt *c*. This protein promotes the assembly of a caspase-activating complex to induce cell apoptosis and stimulates the oxidative stress-induced diseases. Besides the protein also interacts with several other proteins such as cytochrome *c* oxidase, cytochrome *c* reductase included cytochrome *c* peroxidase, cytochrome $b_5$, and Apaf-1 [23–29].

Based on these experimental results, protein–protein docking studies were performed to investigate possible binding mode of human AChE (hAChE, PDB ID: 1B41) with human Cyt *c* (hCyt *c*, PDB ID: 1J3S). Furthermore, two molecular dynamics (MD) simulations were carried out to refine the binding mode of docked structure and to investigate the structural difference in the absence (Apo) and presence (Holo) of heme in the Cyt *c*. In this study, we provide detailed binding modes for both systems with key interacting residues at interface region between hAChE and hCyt *c*.

## 2. Methods

### 2.1. Preparation of 3D structures and sequence analysis

The structures of hAChE (PDB ID: 1B41, 2.76 Å resolution) and hCyt *c* (PDB ID: 1J3S) which are available from Protein Data Bank (http://www.rcsb.org) were taken for protein–protein docking study. Each structure was modified and refined using the *Clean protein* tool of Discovery Studio 2.5 (DS2.5) which corrects incomplete or nonstandard residues and modifies the termini [30]. AChE sequences from four species such as *Homo sapiens* (PDB ID: 1B41), *Mus musculus* (PDB ID: 1MAA), *Torpedo californica* (PDB ID: 1EA5), and *Drosophila melanogaster* (PDB ID: 1QO9), and Cyt *c* sequences from *homo sapiens* (PDB ID: 1J3S) and *Equus cabllus* (PDB ID: 1HRC) were used in multiple sequence alignment using ClustalW2 (http://www.ebi.ac.uk/Tools/clustalW2).

### 2.2. Protein–protein docking study

DOT (Daughter of Turnip) 2.0 is a program for docking of macromolecules that performs a complete, systematic rigid-body search of one molecule translated and rotated about a second molecule. This program has been successfully applied to stable protein–protein interactions, to the transient interactions between electron-transfer proteins, and to protein–DNA interactions [31–33]. This program was used for calculation of protein–protein interaction between hAChE and hCyt *c*, considering former protein as stationary molecule and the later one as moving molecule. A set of 54,000 rotational orientations provided a resolution of 6° for the rotational search. Almost 54,000 different translated orientations of hCyt *c* was obtained about the stationary protein hAChE which was enclosed in an implicitly solvated point grid of dimension $160 \times 160 \times 160$. The Electrostatic potentials (ESPs) were calculated on this grid by UHBD (University of Houston Brownian Dynamics). The rotational and translational search resulted in over 221 billion configurations

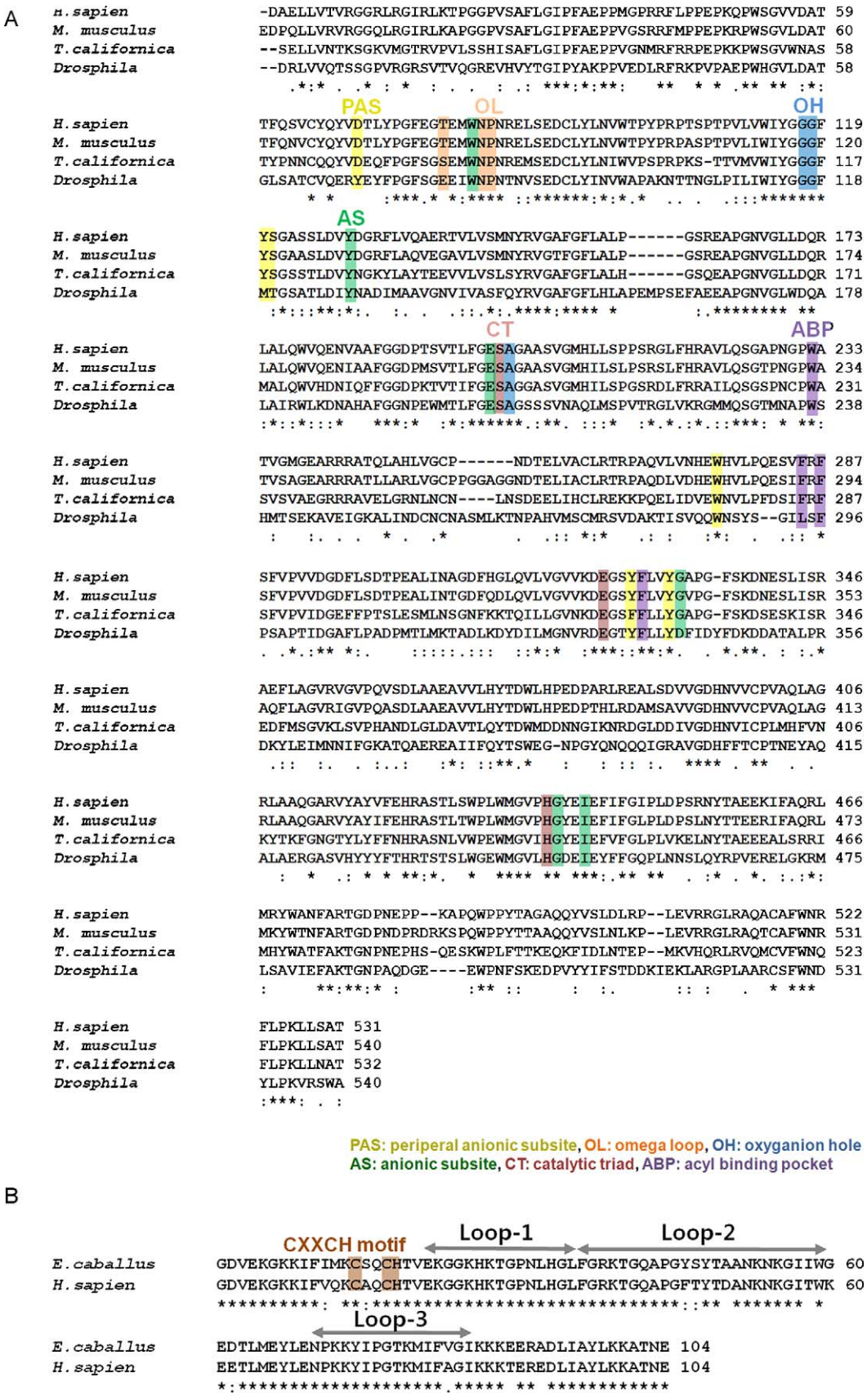


**Fig. 2.** Sequence alignment results for AChE and Cyt *c*. (A) Multiple sequence alignment for AChE of different species. (B) Sequence alignment result between *homo sapiens* Cyt *c* and *Eguus caballus* Cyt *c*. These alignments were generated using ClustalW2 program with the conserved residues indicated with asterisks (*). Subsite and key residues are highlighted with different colors; PAS is highlighted with yellow color, OL with orange, OH with blue, AS with green, CT with magenta, ABP with violet, and CXXCH motif is in brown color. The loop region sequences are indicated by bidirectional arrow. (For interpretation of the references to color in this figure legend, the reader is referred to the web version of the article.)

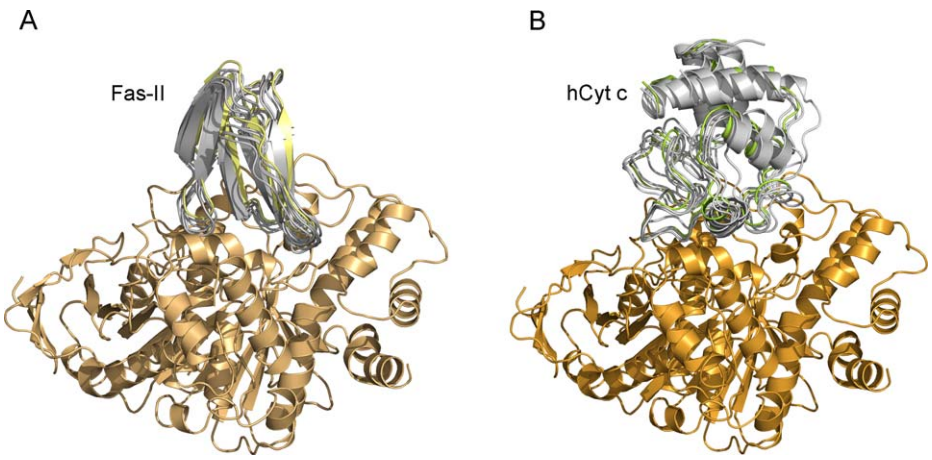


**Fig. 3.** Docked conformations of Fas-II and hCyt *c*. (A) The best Fas-II placement (light yellow) is selected from the top-ranked DOT solutions (grey) docked to the hAChE (light orange). (B) Among the hCyt *c* solutions (grey) docked to the hAChE (orange), the selected structure is represented in light green color. (For interpretation of the references to color in this figure legend, the reader is referred to the web version of the article.)

($160 \times 160 \times 160 \times 54{,}000$) for the two proteins. Long-range and short-range interactions can be examined, because the DOT 2.0 program can perform a complete search.

### 2.3. Molecular dynamics simulation

Molecular dynamics (MD) simulation is needed to provide flexibility and refinement to the docked protein complex because the DOT program uses rigid molecules for its calculation. Two MD simulations were carried out using the GROMACS program (version 3.3.1) [34,35] with GROMOS96 force field for Apo and Holo systems. The initial structures were inserted to an orthorhombic water box (1 nm thickness). The systems were neutralized by the addition of 2 $Cl^-$ counterions for Apo system and 1 $Na^+$ for Holo system. Long range electrostatics was deal by the particle mesh Ewald (PME) method [36]. The proteins alone consists of 6411 atoms and the entire system is made up of 65,114 atoms containing 19,568 water molecules. The steepest descent energy minimization was performed to remove possible bad contacts from the initial structures until energy convergence reached 2000 kJ/(mol nm). The systems were subject to equilibration at 300 K and normal pressure constant (1 bar) for 100 ps under the conditions of position restraints for heavy atoms and LINCS constraints for all bonds. For two systems considered for study, we carried out 10 ns production run under periodic boundary conditions with NPT ensemble. Cutoff distances for the calculation of the electrostatic and Lennard–Jones interaction were 0.9 and 1.4 nm, respectively. The time step of the simulation was set to 2 fs, and the coordinates were saved for analysis every 1 ps. All the analyses of MD simulations were carried out using GROMACS package.

### 2.4. Analysis of protein–protein interaction

The ESP surfaces for the docked protein complexes were calculated using APBS and visualized in PyMOL [37] and the ESP surface for the contours from −1 kT/e (red) to +1 kT/e (blue) were visualized and the dielectric constants of 80 and 2 were used for the solvent and the protein, respectively. PROTORP program [33] was employed to analyze the properties of interface between hAChE and hCyt *c*. This program is a protein–protein interface analysis server and a tool for analyzing the properties of interfaces in the 3D structures of protein–protein associations. DS2.5 package was utilized to find out key residues for hydrogen bonding within 2.5 Å and to detect cation-π interaction among two proteins.

## 3. Results and discussion

### 3.1. Structural and sequence analyses for hAChE and hCyt c

The hAChE (PDB ID: 1B41, 5-543 residues) and hCyt *c* (PDB ID: 1J3S, 1–104 residues) crystal structures were used to perform protein–protein docking simulation. The entire sequence of

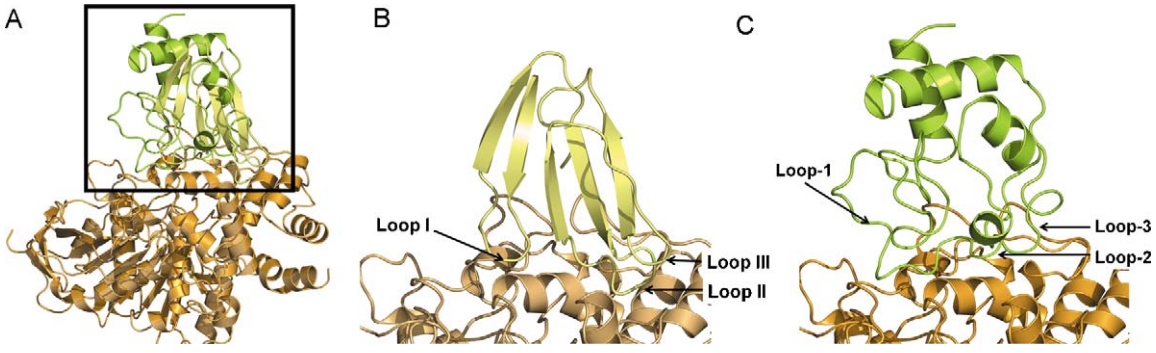


**Fig. 4.** Comparison of the selected conformation with the crystal structure. (A) The selected conformation of hAChE/hCyt *c* complex and the crystal structure of hAChE/Fas-II complex were superimposed to show the similarity of predicted interface region for hCyt *c* with original Fas-II binding site on hAChE. The interface region highlighted by the box is zoomed in (B) and (C), separately. (B) The crystal structure of the complex between hAChE (light orange) and Fas-II (light yellow). (C) The selected conformation of the complex between hAChE (orange) and hCyt *c* (green). The interacting loops were labelled to compare the both binding conformations. (For interpretation of the references to color in this figure legend, the reader is referred to the web version of the article.)

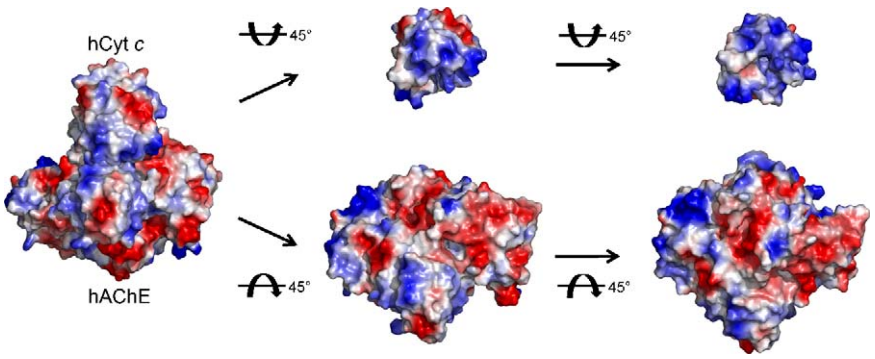


**Fig. 5.** Electrostatic potential (ESP) surfaces of the hCyt *c* with the hAChE. The docked hAChE/hCyt *c* complex structure (left) was represented as ESP surface. The hCyt *c* (upper) and the hAChE (lower) structures are successively rotated by 45 degrees for clarity. The surface model shows the charge-based surface interaction between the proteins hCyt *c* and the hAChE, representing the positive (blue) and negative (red) charges. Both the normal view (left side) and 90°-rotated view (right side) show that the positively charged surface of the hCyt *c* interacts with the negatively charged surface of the hAChE. (For interpretation of the references to color in this figure legend, the reader is referred to the web version of the article.)

hAChE consists of 614 amino acid residues, but the crystal structure contains 531 residues (Asp5-Thr543) excluding N-terminal signal peptide and C-terminal domain residues.

Before proceeding to the main protein–protein docking simulation, structural superimposition and multiple sequence alignment were employed to give some introductions for the both structures. The superimposition among AChE structures was carried out to examine the similarity of the AChE structures with four different species such as *homo sapiens*, *Mus musculus*, *Torpedo californica*, and *Drosophila melanogaster*. From the structural analysis, similar conformation patterns were identified (Fig. 1C). In addition, the multiple sequence alignment of AChE proteins was also performed with the species. Although the lower conservation of total sequence was observed with 30.1% identity and 52.6% similarity, active site residues of AChE were highly conserved in these species (Fig. 2A). The AChE sequence comparison between *homo sapiens* and *Mus musculus* has revealed that they were close to each other with 83.3% and 95.9% of sequence identity and similarity, respectively. Additionally, the sequence alignment between hCyt *c* and *Eguus caballus* Cyt *c* was carried out and it showed 87.6% identity and 92.4% similarity (Fig. 2B). The Cyt *c* consists of 104 amino acid residues including six β-turns and five α-helices. The three conserved helices core which is forming a basket around the heme group [38,39]. Here, the four flexible regions of Cyt *c* called loop-1 (21–35 residues), loop-2 (36–59 residues), loop-3 (70–85 residues), and C-terminal helix regions are denoted based on Singh et al. [40]. The 3D structure has CXXCH motif (Cys14, Cys17, and His18) to bind with heme group and Met80 residue is important to interact with Fe in heme (Fe···S) (Fig. 1D) [41].

### 3.2. Prediction of complex structure of hAChE/hCyt c

To investigate the reasonable interaction between hAChE and hCyt *c*, protein–protein docking studies were carried out using DOT 2.0 macro-molecular docking program. To validate our docking protocol whether the DOT program and considered energy terms are reliable to use for this protein, we performed the macro-molecular docking between hAChE and Fas-II in reported crystal structure (PDB ID: 1B41). The docked conformation of hAChE/Fas-II complex was compared with the previous crystal structure of hAChE/Fas-

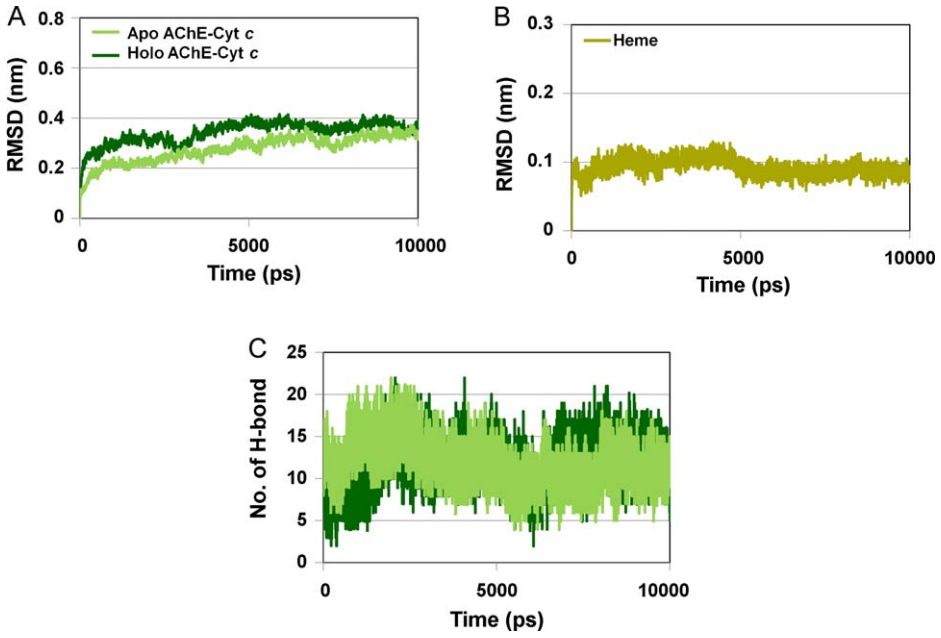


**Fig. 6.** Stability of the complex structure for hAChE/hCyt *c* complex in Apo (hight green) and Holo (dark green) systems. (A) The backbone RMSD of overall hAChE/hCyt *c* complex. (B) The RMSD of heme (yellow) in Holo system. (C) Total number of H-bonds between hAChE and hCyt *c*. (For interpretation of the references to color in this figure legend, the reader is referred to the web version of the article.)

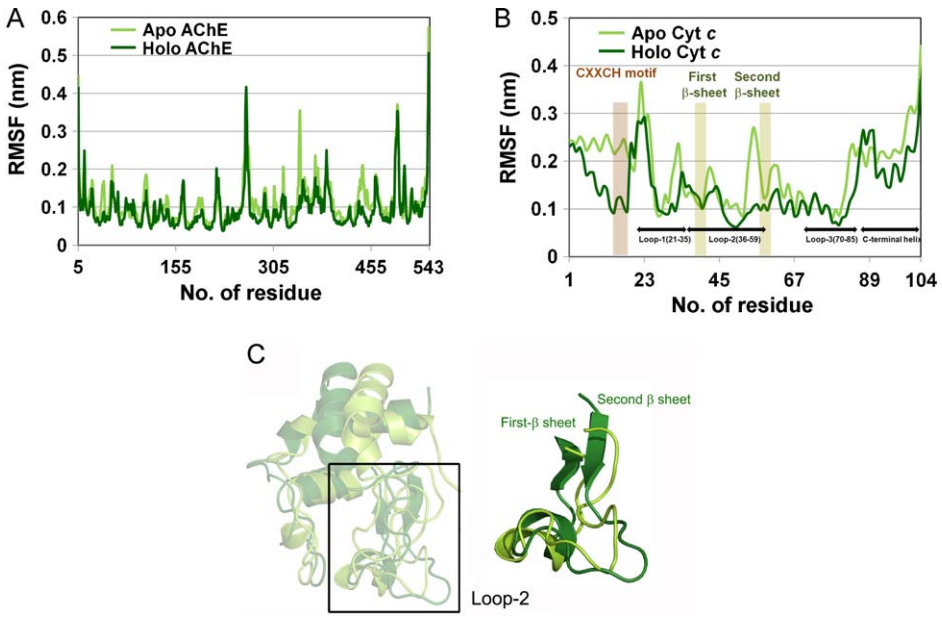


**Fig. 7.** Effect of heme on structural changes. The RMSFs for each protein with respect to residues in the Apo (light green) and Holo (dark green) systems. (A) The RMSFs of hAChE and (B) hCyt *c* of both systems. (C) The representative structures obtained from 10 ns MD simulations were superimposed to investigate the structural change of hCyt *c* by heme group. The detailed view (right side) of the loop-2 region highlighted by box showed that the two β-sheets were formed in Holo system. (For interpretation of the references to color in this figure legend, the reader is referred to the web version of the article.)

II complex. The binding pattern of the docked conformation was similar to the crystal structure conformation (Fig. 3). The result of the docking simulation showed that the docking protocol was reasonable in investigating the binding conformation accurately.

Subsequently, protein–protein docking simulation between hAChE and hCyt *c* was executed considering prior protein as stationary molecule and the later one as moving molecule. Among the DOT solutions, the best 2000 structures were reevaluated with

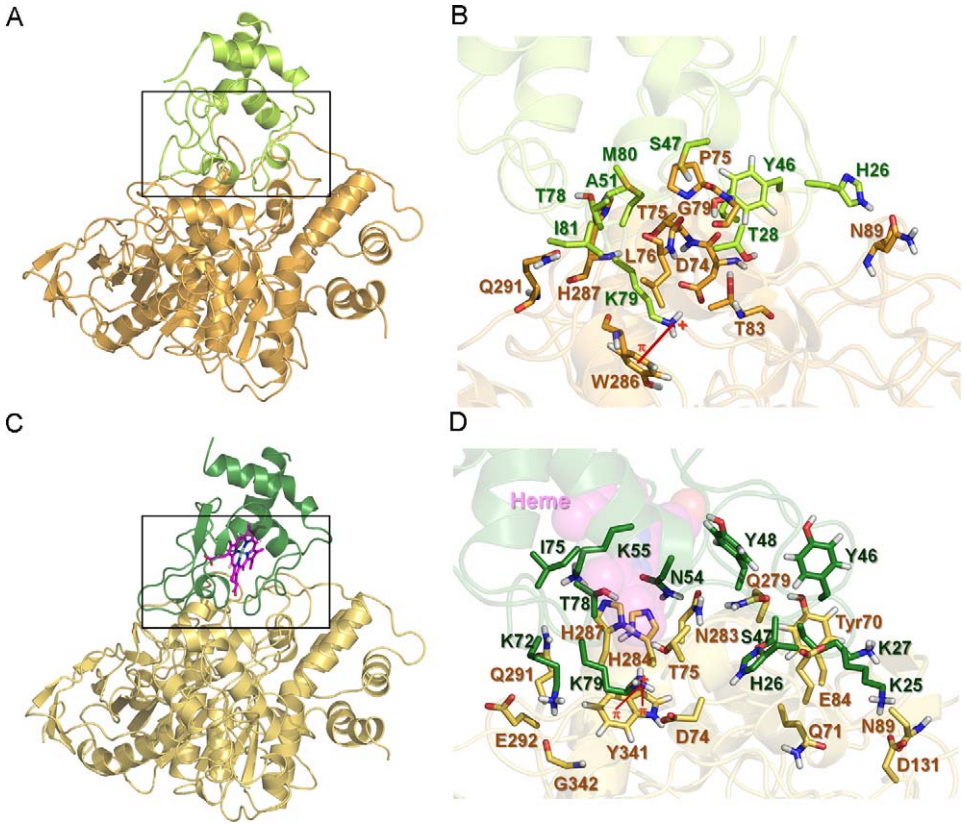


**Fig. 8.** Comparison of hydrogen bonding residues. The representative structures of Apo (A) and Holo (C) systems are shown in cartoon. (B) and (D) show the detailed view of the panels (A) and (C), respectively, with the hydrogen bonding residues between hAChE and hCyt *c*. The heme (magenta) and hydrogen bonding residues are represented as stick model.

**Table 1**
Hydrogen bond and π interaction comparison between hAChE and hCyt *c*.

| Systems | Hydrogen bond interacting residues (hAChE–hCyt *c*) | | Distance (Å) | Cation–π interacting residues (hAChE–hCyt *c*) | | Distance (Å) |
|---|---|---|---|---|---|---|
| Apo | ASP74:O | TYR46:HH | 1.65 | TYR341 | LYS79:NZ | 3.86 |
| | ASP74:OD2 | LYS79:HZ3 | 2.31 | | | |
| | ASP74:OD1 | LYS79:HZ3 | 2.00 | | | |
| | THR75:O | GLY29:H | 2.37 | | | |
| | THR75:OG1 | LYS79:H | 2.21 | | | |
| | THR75:OG1 | MET80:H | 2.14 | | | |
| | LEU76:O | ILE81:H | 2.07 | | | |
| | PRO78:O | CYS17:HG | 1.85 | | | |
| | GLY79:H | THR28:O | 1.98 | | | |
| | THR83:HG1 | THR28:OG1 | 2.07 | | | |
| | ASN89:O | HIS26:HE2 | 2.20 | | | |
| | HIS287:HE2 | ALA51:O | 2.16 | | | |
| | GLN291:OE1 | GLY77:H | 2.10 | | | |
| | GLN291:OE1 | THR78:H | 1.96 | | | |
| | GLN291:HE22 | THR78:O | 2.14 | | | |
| Holo | TYR70:OH | TYR46:H | 2.50 | TRP286 | LYS79:NZ | 4.81 |
| | GLN71:O | SER47:HG | 1.77 | | | 5.22 |
| | ASP74:O | HIS26:HE2 | 2.00 | | | |
| | ASP74:OD2 | LYS79:HZ2 | 2.49 | | | |
| | THR75:OG1 | LYS79:HZ3 | 2.40 | | | |
| | THR75:O | LYS79:HZ1 | 2.37 | | | |
| | GLU84:OE2 | LYS25:H | 1.98 | | | |
| | ASN89:O | LYS27:HZ3 | 2.14 | | | |
| | ASP131:OD2 | LYS25:HZ1 | 2.43 | | | |
| | GLN279:HE22 | TYR48:O | 2.48 | | | |
| | GLN279:OE1 | TYR48:H | 2.37 | | | |
| | ASN283:HD22 | TYR48:O | 1.96 | | | |
| | HIS284:NE2 | ASN54:HD22 | 2.07 | | | |
| | HIS287:NE2 | LYS55:HZ3 | 2.30 | | | |
| | GLN291:HE21 | LYS72:O | 2.19 | | | |
| | GLN291:HE22 | ILE75:O | 2.09 | | | |
| | GLN291:HE21 | THR78:O | 2.11 | | | |
| | GLU292:OE1 | LYS72:HZ1 | 2.21 | | | |
| | GLY342:O | LYS72:HZ2 | 2.41 | | | |

ACE (pairwise atomic contact energy) score. The ACE is the free energy necessary to replace two residue–water contacts by the corresponding residue–residue and water–water contacts [42]. The most of results were located in similar position, and the best placement was selected by the energy scores including electrostatic, van der waals, and ACE (Fig. 3B). The selected hAChE/hCyt *c* complex structure was compared with crystal structure of hAChE/Fas-II complex. The both complexes were superimposed by the hAChE protein and then the interaction region of hCyt *c* was compared with that of Fas-II. Interestingly, the result showed that hCyt *c* was bound to the equivalent binding region of Fas-II (Fig. 4). Generally, several studies reported that Fas-II binds to PAS on AChE [43–45] (Fig. 4B). Based on these results, we can be concluded that hCyt *c* binds to PAS of the hAChE (Fig. 1A and C). From the comparison of interacting loops between Fas-II and Cyt *c*, each loop of Fas-II has similar binding pattern with that of Cyt *c*. As both docking structures were placed at same position, similar interacting residues of AChE were observed in the two binding conformations. Electrostatic potential (ESP) surfaces of docked hAChE/hCyt *c* complex were examined to check the reliability of the selected structure. The differences in the ESP surfaces of the hAChE and hCyt *c* are clearly described by 45 degrees rotations, opposite direction of each protein (Fig. 5). The ESP analysis was disclosed that the hAChE is distributed with negative charge, while hCyt *c* displays positive charge in the interacting region. Moreover, the exposed part of hCyt *c* was properly fitted into the deep cleft of hAChE. Finally, the reasonable structure complex of hAChE/hCyt *c* was obtained, and the complex conformation was used for MD simulation.

### *3.3. Stability of the complex structure in each system with and without heme*

MD simulations were carried out (i) to refine the docked complex structure because the DOT program uses rigid molecules for its calculation and (ii) to observe the differences of the binding conformations by comparing between systems with and without heme. The Cyt *c* containing heme can trigger Apaf-1 dependent caspase activation by binding to Apaf-1, but apo Cyt *c* inhibits caspases by preventing apoptosome formation [46]. While the evidence of interaction between Apaf-1 and Cyt *c* has been reported, there is no information for interaction of AChE with Cyt *c* including heme group or not. Hence, two 10 ns MD simulations for the complex of hAChE/hCyt *c* were performed with and without heme group in hCyt *c*, which are named as Apo and Holo systems, respectively.

To confirm the stability of the simulations, backbone root mean square deviations (RMSD) and number of hydrogen bonds between hAChE and hCyt *c* were analyzed during 10 ns simulation time. The Apo system gradually increased up to 0.4 nm and then achieved stability after approximately 7900 ps, but Holo system has reached the stability after about 3900 ps. Although the fluctuation of Holo was higher than Apo system, the RMSD of Holo was maintained about 0.37 nm until 10 ns (Fig. 6A). From the RMSD analysis for heme in the Holo system, we observed that heme was constantly stable after around 5000 ps (Fig. 6B). Moreover, H-bonds analysis showed that Holo system has more H-bonds than Apo after 6500 ps (Fig. 6C). These results showed that structural stability of the both complexes was well converged in similar level. Moreover, the results

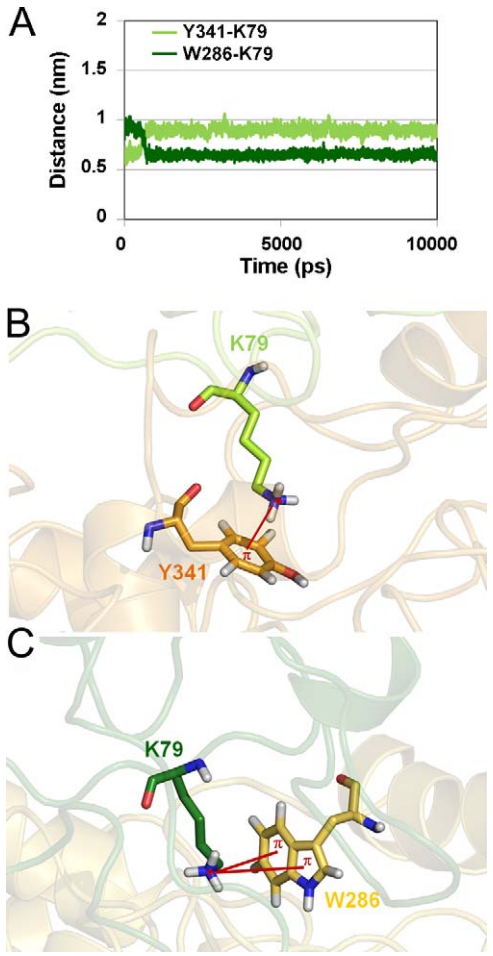


**Fig. 9.** Cation-π interaction between hAChE and hCyt *c* in the two systems. (A) The distance between key residues which were contributed to cation-π interaction in both systems (light green for Apo and dark green for Holo system). The interaction of the key residues in the Apo (B) and Holo (C) systems. The cation-π interaction indicated by the red line and π and + are marked for pi and cation, respectively. (For interpretation of the references to color in this figure legend, the reader is referred to the web version of the article.)

suggest that our MD simulation is dependable to reproduce the overall conformational dynamics.

### 3.4. Comparison of structural behaviours and flexibilities between the two systems

To observe the differences of structural behaviours and flexibilities in the proteins of two systems, representative structures and root mean square fluctuation (RMSF) graphs for each system were analyzed and compared (Fig. 7). The representative structures of hAChE/hCyt *c* complex were selected by considering the closest snapshot with average structure during last 2 ns (from 8000 ps to 10,000 ps). The selected snapshots (9344 ps snapshot for Apo and 9226 ps snapshot for Holo) were utilized to analyze all qualitative data in this study.

The hAChE was not detected with any noticeable aspect of conformational change (Fig. 7A) whereas hCyt *c* has displayed conspicuous structural change, especially in loop-2 (Fig. 7B). The two β-sheets (38–41 residues for first β-sheet and 57–60 for second β-sheet) were formed in loop-2 region of hCyt *c* in Holo system (Figs. 1D and 7C). From the RMSF analysis for the loop, although the loop-2 is highly flexible in Apo system, the low flexibility of the loop-2 in Holo system was induced by the forming of β-sheets (Fig. 7B and C). The hCyt *c* has CxxCH (Cys14, Cys17, and His18) motif which is known as heme binding sites. The interaction of these three residues with the heme group was investigated from the representative structure and the Met80 has also formed Fe···S bond with heme iron. The RMSF analysis showed that the motif region of Holo system has lower flexibility than Apo system by the presence of heme group. These interactions affected the rigidity of the motif region in Holo system.

**Table 2**
Protein–protein interaction comparison between AChE and Cyt *c*.

| System | No. of H-bond interaction | No. of cation-π interaction | Interface accessible surface area (Å$^2$) |
|---|---|---|---|
| Apo | 15 | 1 | 1219.43 |
| Holo | 19 | 2 | 1263.52 |

According to the other MD simulation studies for eukaryotic holo Cyt *c*, the entire structure of the Cyt *c* has shown the high flexibility and low stability [40,47,48]. However, our results showed an opposite trend, this difference was caused by the presence of hAChE interacting with the flexible loops in hCyt *c*.

### 3.5. Interacting residues between hAChE and hCyt c proteins in the two systems

To investigate interacting residues between two proteins hAChE and hCyt *c*, structural analyses were carried out using DS2.5 to detect hydrogen bonding residues (Fig. 8). From the H-bond analysis, residues at the interface region residues (Asp74, Thr75, Leu76, Pro78, Gly79, Thr83, Asn89, His287, and Gln291) of hAChE were observed to interact by hydrogen bonding with following residues of hCyt *c* in Apo system: Cys17, His26, Thr28, Gly29, Tyr46, Ala51, Gly77, Thr78, Lys79, Met80, and Ile81 (Table 1, Fig. 8A and B). In Holo system, Tyr70, Gln71, Asp74, Thr75, Glu84, Asn89, Asp131, Gln279, Asn283, His284, His287, Gln291, Glu292, and Gly342 of hAChE interact with Lys25, His26, Lys27, Tyr46, Ser47, Tyr48, Asn54, Lys55, Lys72, Ile75, Thr78, and Lys79 of hCyt *c* through hydrogen bonding interaction (Table 1, Fig. 8C and D). Whereas the Thr75 and Pro78 residues of hAChE in the Apo system have formed H-bonds with Met80 and Cys17 of hCyt *c*, respectively, these interactions in the Holo system were not observed because Met80 and Cys17 residues were found to be involved in heme binding. This difference between Apo and Holo systems is induced by the presence or absence of heme group in the hCyt *c*.

### 3.6. Cation-π interactions between hAChE and hCyt c proteins in the two systems

Using *Pi Interactions* options in DS2.5, cation-π interactions between hAChE and hCyt *c* were identified (Fig. 9). The cation-π interaction is a strong, general, and noncovalent binding interaction. These interactions are possible to occur between aromatic amino acid such as phenylalanine, tyrosine, and tryptophan as the π component and lysine or alanine as the cation [49,50]. Several studies have showed that cation-π interaction plays an important role in the stability of protein structures [51–53] and the interaction is considered as an significant contributor to protein–protein interfaces [54].

The stronger cation-π interaction was observed in Holo system than the Apo system, with maintaining stable distance between 0.7 and 0.9 nm for Holo and Apo systems, respectively (Fig. 9A). The cation-π interaction between Tyr341 residue of AChE and Lys79 residue of Cyt *c* was observed in Apo system (Fig. 9B, Table 1). To the contrary, the two cation-π interactions were observed in Holo system, and the aromatic residue which is contributed to the interaction as π component was Trp instead of Tyr residue. The Trp286 residue of hAChE participated in cation-π interaction with Lys79

residue of hCyt *c* (Fig. 9C, Table 1). Consequently, the two aromatic amino acids of hAChE, namely, Tyr341 and Trp286 are considered as important residues for protein–protein interaction. Especially, the Lys79 of hCyt *c* also might be one of the key residues to the interaction.

The interface interactions of the Holo system including H-bonds and cation-π as well as interface accessible surface area (1219.43 Å for Apo and 1263.52 Å for Holo) are stronger and larger than those of the Apo system (Table 2). These results suggested that overall interaction between hCyt *c* and hAChE of Holo system is stronger than that of Apo system.

## 4. Conclusions

The ultimate aim of this study was to predict the binding conformation between hAChE and hCyt *c*. The macro-molecular docking and MD simulations were successfully performed to investigate the reasonable binding conformation. The best docked conformation was selected by the energy scores including electrostatic, van der waals, and ACE and then evaluated by structural comparison and ESP calculation. The final docked conformation showed that the hCyt *c* was bound to PAS of hAChE. From the two 10 ns MD simulations with and without heme group, we observed that both systems have similar binding pattern, but several differences were also observed. In the RMSF analysis, although the loop-2 is highly flexible in Apo system, the low flexibility of the loop-2 in Holo system was induced by the forming of β-sheets. The CxxCH motif region of Holo system has lower flexibility than Apo system by the presence of heme group. The H-bond and cation-π interactions and interface accessible surface area of Holo system were stronger and larger than those of the Apo system. Therefore, this study demonstrated that interaction between hCyt *c* and hAChE of Holo system was more stable than that of Apo system. The key hydrogen bonding residues between hAChE and hCyt *c* proteins were observed in each system. Moreover, Tyr341 and Trp286 of hAChE were found to have cation-π interaction with Lys79 of hCyt *c*. In conclusion, our study provides detailed binding modes for both systems with key interacting residues at interface region between hAChE and hCyt *c*.

## Acknowledgements

This research was supported by Basic Science Research Program (2009-0073267), Fundamental Technology Development Program (2009-0081539), and Big Sciecne R&D Program (2010-0029084) through the National Research Foundation of Korea (NRF) funded by the Korean Government (MEST). And all students were recipient of fellowship from the BK21 Program of MEST.

## References

[1] P. Taylor, Z. Radic, The cholinesterases: from genes to proteins, Annu. Rev. Pharmacol. Toxicol. 34 (1994) 281–320.
[2] D. Small, S. Michaelson, G. Sberna, Non-classical actions of cholinesterases: role in cellular differentiation, tumorigenesis and Alzheimer's disease, Neurochem. Int. 28 (1996) 453–483.
[3] D. Grisaru, M. Sternfeld, A. Eldor, D. Glick, H. Soreq, Structural roles of acetylcholinesterase variants in biology and pathology, Eur. J. Biochem. 264 (1999) 672–686.
[4] H. Soreq, S. Seidman, Acetylcholinesterase—new roles for an old actor, Nat. Rev. Neurosci. 2 (2001) 294–302.
[5] C. Legay, M. Huchet, J. Massoulie, J. Changeux, Developmental regulation of acetylcholinesterase transcripts in the mouse diaphragm: alternative splicing and focalization, Eur. J. Neurosci. 7 (1995) 1803–1809.
[6] Y. Dudai, M. Herzberg, I. Silman, Molecular structures of acetylcholinesterase from electric organ tissue of the electric eel, Proc. Natl. Acad. Sci. U.S.A. 70 (1973) 2473.
[7] F. Rieger, S. Et, J. MassouliE, J. Cartaud, Observation par microscopie electronique des formes allongees et globulaires de l'acetylcholinesterase de gymnote (Electrophorus electricus), Eur. J. Biochem. 34 (1973) 539–547.
[8] H. Dvir, M. Harel, S. Bon, W.Q. Liu, M. Vidal, C. Garbay, et al., The synaptic acetylcholinesterase tetramer assembles around a polyproline II helix, EMBO J. 23 (2004) 4394–4405.
[9] H. Dvir, H. Jiang, D. Wong, M. Harel, M. Chetrit, X. He, et al., X-ray structures of torpedo californica acetylcholinesterase complexed with (+)-huperzine A and (−)-huperzine B: structural evidence for an active site rearrangement, Biochemistry 41 (2002) 10810–10818.
[10] M. Harel, G. Kryger, T. Rosenberry, W. Mallender, T. Lewis, R. Fletcher, et al., Three-dimensional structures of Drosophila melanogaster acetylcholinesterase and of its complexes with two potent inhibitors, Protein Sci. 9 (2000) 1063–1072.
[11] Y. Bourne, P. Taylor, P.E. Bougis, P. Marchot, Crystal structure of mouse acetylcholinesterase. A peripheral site-occluding loop in a tetrameric assembly, J. Biol. Chem. 274 (1999) 2963–2970.
[12] G. Kryger, M. Harel, K. Giles, L. Toker, B. Velan, A. Lazar, et al., Structures of recombinant native and E202Q mutant human acetylcholinesterase complexed with the snake-venom toxin fasciculin-II, Acta Crystallogr. D: Biol. Crystallogr. 56 (2000) 1385–1394.
[13] P. Taylor, S. Lappi, Interaction of fluorescence probes with acetylcholinesterase. The site and specificity of propidium binding, Biochemistry 14 (1975) 1989–1997.
[14] J. Wang, J. Gu, J. Leszczynski, Hydrogen-bonding interactions in the binding of loop 1 of fasciculin 2 to Torpedo californica acetylcholinesterase: a density functional theory study, J. Phys. Chem. B 109 (2005) 13761–13769.
[15] J. Wiesner, Z. Ki, K. Kua, D. Jun, J. Koa, Acetylcholinesterases—the structural similarities and differences, J. Enzyme Inhib. Med. Chem. 22 (2007) 417–424.
[16] M. Khan, Molecular interactions of cholinesterases inhibitors using in silico methods: current status and future prospects, Nat. Biotechnol. 25 (2009) 331–346.
[17] G. Mooser, D.S. Sigman, Ligand binding properties of acetylcholinesterase determined with fluorescent probes, Biochemistry 13 (1974) 2299–2307.
[18] J.P. Changeux, Responses of acetylcholinesterase from Torpedo marmorata to salts and curarizing drugs, Mol. Pharmacol. 2 (1966) 369.
[19] F. Bergmann, I.B. Wilson, D. Nachmansohn, The inhibitory effect of stilbamidine, curare and related compounds and its relationship to the active groups of acetylcholine esterase. Action of stilbamidine upon nerve impulse conduction, Biochim. Biophys. Acta 6 (1951) 217–224.
[20] X. Zhang, L. Yang, Q. Zhao, J. Caen, H. He, Q. Jin, et al., Induction of acetylcholinesterase expression during apoptosis in various cell types, Cell Death Differ. 9 (2002) 790.
[21] S.E. Park, N.D. Kim, Y.H. Yoo, Acetylcholinesterase plays a pivotal role in apoptosome formation, Cancer Res. 64 (2004) 2652–2655.
[22] S. Park, S. Jeong, S. Yee, T. Kim, Y. Soung, N. Ha, et al., Interactions of acetylcholinesterase with caveolin-1 and subsequently with cytochrome c are required for apoptosome formation, Carcinogenesis 29 (2008) 729.
[23] S.M. Khan, D.S. Cassarino, N.N. Abramova, P.M. Keeney, M.K. Borland, P.A. Trimmer, et al., Alzheimer's disease cybrids replicate beta-amyloid abnormalities through cell death pathways, Ann. Neurol. 48 (2000) 148–155.
[24] Y. Shi, A structural view of mitochondria-mediated apoptosis, Nat. Struct. Biol. 8 (2001) 394–401.
[25] J.W. Allen, M.L. Ginger, S.J. Ferguson, Complexity and diversity in c-type cytochrome biogenesis systems, Biochem. Soc. Trans. 33 (2005) 145–146.
[26] A. Jungst, S. Wakabayashi, H. Matsubara, W. Zumft, The nirSTBM region coding for cytochrome cd1-dependent nitrite respiration of Pseudomonas stutzeri consists of a cluster of mono-, di-, and tetraheme proteins, FEBS Lett. 279 (1991) 205–209.
[27] P. Hamel, V. Corvest, P. Giege, G. Bonnard, Biochemical requirements for the maturation of mitochondrial c-type cytochromes, Biochim. Biophys. Acta 1793 (2009) 125–138.
[28] C. Adrain, S.J. Martin, The mitochondrial apoptosome: a killer unleashed by the cytochrome seas, Trends Biochem. Sci. 26 (2001) 390–397.
[29] R.M. Kluck, E. Bossy-Wetzel, D.R. Green, D.D. Newmeyer, The release of cytochrome c from mitochondria: a primary site for Bcl-2 regulation of apoptosis, Science 275 (1997) 1132–1136.
[30] D. Studio, Version 2.1, Accelrys Inc., San Diego, CA, 2009.
[31] A.A. Adesokan, V.A. Roberts, K.W. Lee, R.D. Lins, J.M. Briggs, Prediction of HIV-1 integrase/viral DNA interactions in the catalytic domain by fast molecular docking, J. Med. Chem. 47 (2004) 821–828.
[32] J. Mandell, V. Roberts, M. Pique, V. Kotlovyi, J. Mitchell, E. Nelson, et al., Protein docking using continuum electrostatics and geometric fit, Protein Eng. Des. Sel. 14 (2001) 105.
[33] L. Ten Eyck, J. Mandell, V. Roberts, M. Pique, Surveying Molecular Interactions with DOT. Inc. ACM, 1995, p. 22.
[34] H. Berendsen, D. van der Spoel, R. Van Drunen, GROMACS: a message-passing parallel molecular dynamics implementation, Comput. Phys. Commun. 91 (1995) 43–56.
[35] D. Van Der Spoel, E. Lindahl, B. Hess, G. Groenhof, A.E. Mark, H.J. Berendsen, GROMACS: fast, flexible, and free, J. Comput. Chem. 26 (2005) 1701–1718.
[36] T. Darden, D. York, L. Pedersen, Particle mesh Ewald: an *N* log (*N*) method for Ewald sums in large systems, J. Chem. Phys. 98 (1993) 10089.
[37] N. Baker, D. Sept, S. Joseph, M. Holst, J. McCammon, Electrostatics of nanosystems: application to microtubules and the ribosome, Proc. Natl. Acad. Sci. U.S.A. 98 (2001) 10037.

[38] G. Bushnell, G. Louie, G. Brayer, High-resolution three-dimensional structure of horse heart cytochrome c, J. Mol. Biol. 214 (1990) 585–595.
[39] L. Banci, I. Bertini, J.G. Huber, G.A. Spyroulias, P. Turano, Solution structure of reduced horse heart cytochrome c, J. Biol. Inorg. Chem. 4 (1999) 21–31.
[40] S. Singh, S. Prakash, V. Vasu, C. Karunakaran, Conformational flexibility decreased due to Y67F and F82H mutations in cytochrome c: molecular dynamics simulation studies, J. Mol. Graph. Model. 28 (2009) 270–277.
[41] A. Raphael, H. Gray, Semisynthesis of axial-ligand (position 80) mutants of cytochrome c, J. Am. Chem. Soc. 113 (1991) 1038–1040.
[42] C. Zhang, G. Vasmatzis, J. Cornette, C. DeLisi, Determination of atomic desolvation energies from the structures of crystallized proteins1, J. Mol. Biol. 267 (1997) 707–726.
[43] P. Marchot, A. Khelif, Y.H. Ji, P. Mansuelle, P.E. Bougis, Binding of 125I-fasciculin to rat brain acetylcholinesterase. The complex still binds diisopropyl fluorophosphate, J. Biol. Chem. 268 (1993) 12458–12467.
[44] J. Eastman, E.J. Wilson, C. Cervenansky, T.L. Rosenberry, Fasciculin 2 binds to the peripheral site on acetylcholinesterase and inhibits substrate hydrolysis by slowing a step involving proton transfer during enzyme acylation, J. Biol. Chem. 270 (1995) 19694–19701.
[45] T. Szegletes, W.D. Mallender, T.L. Rosenberry, Nonequilibrium analysis alters the mechanistic interpretation of inhibition of acetylcholinesterase by peripheral site ligands, Biochemistry 37 (1998) 4206–4216.
[46] A.G. Martin, J. Nguyen, J.A. Wells, H.O. Fearnhead, Apo cytochrome c inhibits caspases by preventing apoptosome formation, Biochem. Biophys. Res. Commun. 319 (2004) 944–950.
[47] A.M. Berghuis, G.D. Brayer, Oxidation state-dependent conformational changes in cytochrome c, J. Mol. Biol. 223 (1992) 959–976.
[48] A.C. Dong, P. Huang, W.S. Caughey, Redox-dependent changes in beta-extended chain and turn structures of cytochrome c in water solution determined by second derivative amide I infrared spectra, Biochemistry 31 (1992) 182–189.
[49] J. Ma, D. Dougherty, The cation-pi interaction, Chem. Rev. 97 (1997) 1303–1324.
[50] D. Dougherty, Cation-pi interactions in chemistry and biology: a new view of benzene, Phe, Tyr, and Trp, Science 271 (1996) 163.
[51] R. Prajapati, M. Sirajuddin, V. Durani, S. Sreeramulu, R. Varadarajan, Contribution of cation-π interactions to protein stability, Biochemistry 45 (2006) 15000–15010.
[52] R. Wintjens, J. Lievin, M. Rooman, E. Buisine, Contribution of cation-pi interactions to the stability of protein–DNA complexes1, J. Mol. Biol. 302 (2000) 393–408.
[53] M. Gromiha, C. Santhosh, S. Ahmad, Structural analysis of cation-pi interactions in DNA binding proteins, Int. J. Biol. Macromol. 34 (2004) 203–211.
[54] P. Crowley, A. Golovin, Cation-π interactions in protein–protein interfaces, Proteins 59 (2005) 231–239.